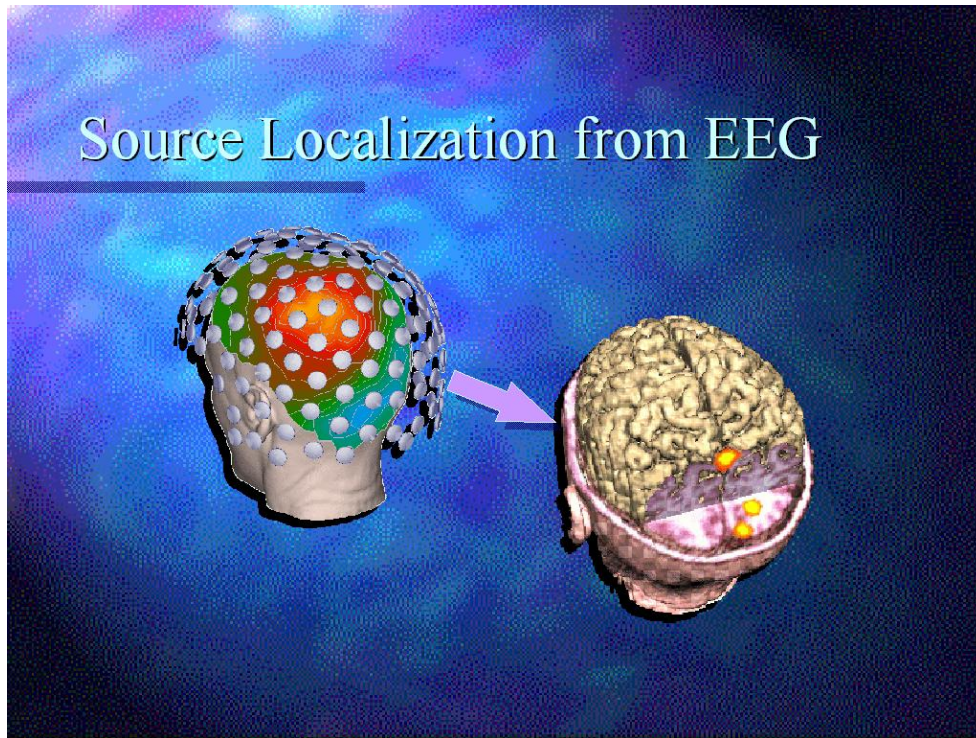# CHALMERS

Source Localization from EEG

Influence of Head Model on EEG Source Localization

Master Thesis of Signals and Systems Department

PRATHAMESH SHARAD DHANPALWAR

XINYUAN CHEN

Influence of Head Model on EEG Source Localization

PRATHAMESH SHARAD DHANPALWAR

Telephone +46(0)735740436

Department of Signals and Systems

XINYUAN CHEN

Telephone +46(0)765833913

Department of Signals and Systems

Supervisor:

YAZDAN SHIRVANY

Chalmers University of Technology

SE-412 96 Göteborg

Sweden

Examiner:

HOI-SHUN LUI

Chalmers University of Technology

SE-412 96 Göteborg

Sweden

Telephone +46(0)317723382

Dedicated

To Parents

&

Everyone Who Have Made This Possible

ABSTRACT

Spike EEG source localization result is influenced by different errors and approximations, e.g., head-model complexity, EEG signal noise, tissue conductivity noise and electrode misplacements. For accurate interpretation of source localization it is crucial to understand the influence of these errors on the source localization results. In this paper the influence of these sources of noise on the EEG source localization were examined in details. Six finite element head models were selected for head-model complexity study. A reference head model was used to create synthetic EEG signals by placing the dipole source inside the model to mimic the epileptic spike signal. For the inverse source localizations an exhaustive search method was used to estimate the best dipole parameters with the EEG signals. Results showed that the inverse problem is significantly influenced by the head-model complexity. A head model with more tissues has better localization results as compared with one with fewer tissues. Moreover, CSF layer plays an important role to achieve an accurate source localization results. To understand the influence of other sources of noise on the EEG source localization, different level of noises were added to EEG signals, tissue conductivities and electrode positions, independently. Simulation results showed that source localization is very sensitive to the tissue conductivity noises. 4% noise on conductivities cause approximately 13mm localization error. Moreover, an electrode misplacement error makes approximately 17% relative error and 8mm localization error for 1cm electrode misplacements. The EEG signal with SNR equal to 6 and higher had an acceptable localization error.

Keywords: - *epilepsy, inverse problem, and source localization.*

ACKNOWLEDGEMENTS

Tables of contents

CHAPTER 1 INTRODUCTION

Surgical therapy has become an important therapeutic alternative for patients with medically intractable epilepsy. Correct and anatomically precise localization of the epileptic focus is mandatory to decide if resection of brain tissue is possible. Lot of research and methods have been developed for the non-invasive measurement of the electrical brain activity. The most important diagnosis tool used at epilepsy surgery centers is electroencephalography (EEG), which is used to find the source of activities inside the brain by measuring the voltage potential on the scalp with the EEG electrodes at different locations. The brain activity is often modelled as a current dipole. It is shown[1] that this current dipole is an acceptable approximation for modelling the neural activities in the brain.

The localization of brain sources is vital in different ways and in various areas of medical diagnosis of brain such as clinical neuroscience, epilepsy treatment, etc. As the brain sources are the cause of the potential at the scalp, it can be used to localize the source and also can be used to know the underlying neural activity. Different criteria like modelling the brain's electrical activity, modelling the brain's volume conduction, geometry of the head model, reconstructing the brain's electrical activity in accordance to the EEG are the keys to source localization.

The procedure of the EEG source localization deals with two problems. First, the forward problem to find the scalp potentials for the given current dipole(s) inside the brain, and second the inverse problem to estimate the source(s) that fits with the given potential distribution at the scalp electrodes. Thus, source localization requires an accurate solution of the inverse problem with a realistic computational effort for the forward problem. Source localization is heavily dependent on the choice of dipole model and several different alternatives have been suggested in the literature[2, 3]. Also its accuracy is affected by different factors including, head-modelling complexity, EEG signal noise, tissue conductivity noise, and electrode misplacements.

Understanding the influence of these errors is very important to have source localization as reliable pre-surgical workup. In this project, four parameters were studied. These four parameters are: different head models, signal noise, conductivity noise and segmentation errors. EEG-based source localization is an active field of research[4], but partly due to the mentioned shortcomings the computational techniques are not yet part of the standard pre-surgical diagnostic workup.

Realistic head models of the human brain are quite complex with the tissue

conductivities, which are highly anisotropic and inhomogeneous. The conductivity values of the tissues play a crucial role in the source localization. These conductivities are also associated with respective noise levels and the project throws light on the sensitivity of this noise level on the source localization.

The complexity of the realistic head models of human brain also leads to huge time consumption during forward problem. It is not a big problem. However, it would be better if the time could be decreased. Simplifying the head models could significantly save time, but the accuracy would be lower. As a result, different tissue-component head models were tested to try and obtain the balance between the accuracy and the time consumption.

Another parameter that influences the accuracy of the estimated source position is the segmentation errors. As the human brain is very complex, exact segmentation is highly impossible. The segmentation also plays a crucial role in the source localization process. The subsequent of the tissues is made based on the analysis done through segmentation tools like FMIRB software library (FSL), widely used imaging segmentation software. Thereby, this process is tested by three threshold levels, each segmented by FSL with different threshold values. By this, one can understand the effects of segmentation in the EEG source localization. Therefore, the influence of the segmentation at different thresholds on source localization is studied.

While using EEG to measure the potentials generated by the epilepsy source, the signals are easy to be disturbed by the noise and interference existing in the surrounding environment. Thus, signal noise is another parameter that must be considered to know its influence on the accuracy of the EEG source localization. Various noise levels were applied to carry out this analysis.

The rest of the report is structured as follow: Chapter 2 discusses the challenges and limitations in EEG source localization. Chapter 3 introduces the methodology of this study. The results are given in Chapter 4. In Chapter 5, the results are discussed and finally, in Chapter 6, the conclusions are made.

CHAPTER 2 BACKGROUND

2.1 Aim

The aim of the EEG source localization is to find out the areas of brains that are responsible for brain waves of interest. The aim is achieved by solving two problems. They are forward and inverse problems. The forward problem consists of finding the potentials at the electrodes, which is initiated by the given electrical source. The inverse problem is about finding the source responsible for the obtained electrode potentials by making use of these potentials. During the last two decades, the development in the computational techniques and extensive research had given a new approach in solving the forward and inverse problems[4].

2.2 Forward Problem

2.2.1 Theory

The forward model describes the propagation of current from the source to the scalp. There could be errors in the construction of the volume conductor and the geometry. Thereby, the errors can also cause subsequently in inverse problem also. That is miss localization of the neural source[5].

Historically, concentric nested spheres with homogeneous and isotropic conductivities were assumed to be the most commonly used head model from the modelling point of view and also from solution point of view. But with the due course of the extensive research in solving the forward and inverse problems in the realistic non-spherical head model, various numerical methods were used to model the realistic and the most approximate head model with respect to its shape, heterogeneity, conductivity of tissues[6].

Also, the quasi-static condition is considered as the current in the conducting brain changes with time, but this change takes place very slowly and therefore, seems like a stable state. The wavelength becomes much larger than the radius of the brain. Therefore, it is named as quasi-static condition. The Maxwell equation for the potential can be used to model the quasi-static approximation.

In order to relate the current dipole and the potential at a distance in the conducting medium, Poisson's equation can be used. This equation is developed from the divergence operator. Applying the divergence operator to the vector field $J(x, y, z)$, the flux density of the vector field from an infinitesimal volume around a specific point can be represented. It is

defined as follows[4]:

$$\nabla \cdot \boldsymbol{J} = \lim_{G \to 0} \frac{1}{G} \oint_{\partial G} \boldsymbol{J} d\boldsymbol{S} \tag{1}$$

where $\nabla \cdot \boldsymbol{J}$ is the current source density, $\oint_{\partial G} \boldsymbol{J} d\boldsymbol{S}$ is the flux or a current, $\boldsymbol{S}$ is the area of a closed surface encircling the specific point, and G is the volume of the region delimited by the closed surface.

The current source density can also be symbolized with I_m, which is:

$$\nabla \cdot \boldsymbol{J} = I_m \tag{2}$$

Ohm's law shows the relationship between the current density $\boldsymbol{J}$ and the electric field $\boldsymbol{E}$, which is:

$$\boldsymbol{J} = \sigma \boldsymbol{E} \tag{3}$$

where σ is the conductivity value and can be a position-depended variable.

Due to the quasi-static conditions, Faraday's law equals zero. Therefore, a link between the potential field V and the electric field $\boldsymbol{E}$ can be constructed using the gradient operator:

$$\boldsymbol{E} = -\nabla V \tag{4}$$

The vector ∇V at a point shows the direction where the potential V most rapidly increases, and the minus sign tells the orientation of the electric field is from the high potential area to a low potential area.

Combining all the equations above together, the Poisson's differential equation is obtained. That is:

$$\nabla \cdot \left(\sigma \nabla (V) \right) = -I_m \tag{5}$$

Figure 2.1 below shows the dipole moment and its potential distribution. The figure also shows the polarity of the dipole.
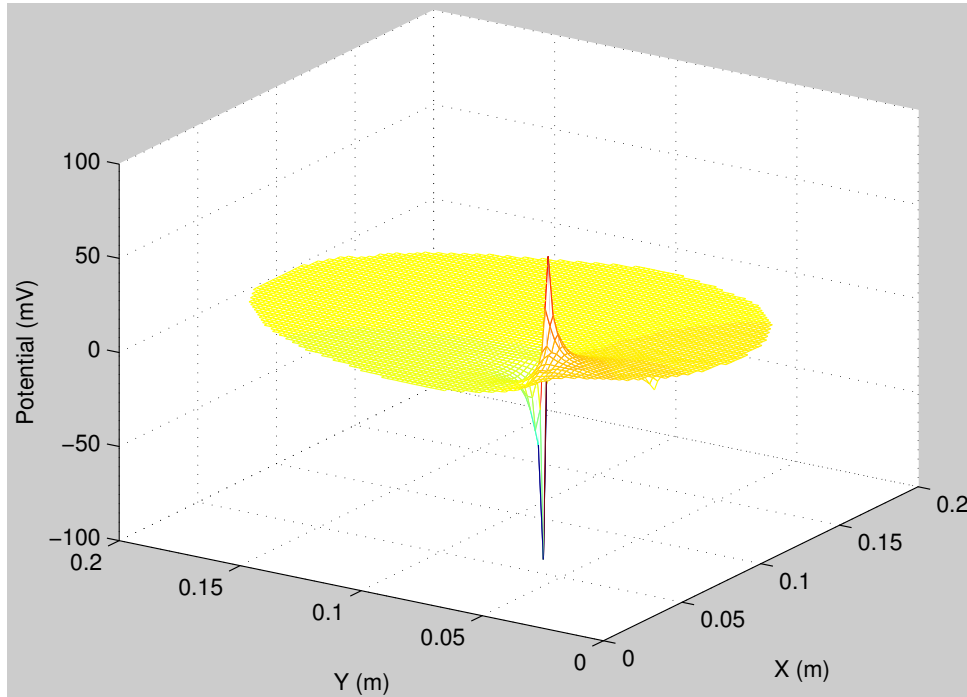
Figure 2.1 Potential distribution of the current dipole

2.2.2 Finite element method (FEM)

Finite Element Method (FEM) is a method for numerical solutions of field problems relying on the development of computer techniques[7]. In 1943, R. Courant applied the piecewise continuous functions in triangular domain[8]. This is thought to be the generation of FEM. This method came into the industry since 1950s, starting from the airframe problem and structural analysis[9]. In 1960, Ray W. Clough first raised the term finite element. In the late 1960s and early 1970s, this method was extensively used to solve different engineering problems[7]. Now, it has become a commonly utilized numerical method in many industries such as aerospace, automotive, chemical, civil, electrical, mechanical, and medical[10].

Many engineering and applied science problems can be described by "governing equations" and "boundary conditions", and partial differential equations (PDE) are common used to express the governing equations and boundary conditions[7]. Nowadays, the engineering problems become more complex than before. It is impossible to use the traditional PDE methods to solve these problems due to the complex geometry and other issues such as the complex properties and boundary solutions. Besides, current product design cycle requires getting the optimized solutions in short time while the traditional PDE methods always cost too much time[11]. Because of the two main problems, engineers consider to perform some approximate solutions instead, which spend acceptable time but can give

reasonable result. FEM is such kind of method.

The fundamental concepts behind the method are given here. In FEM, a system is divided into some small elements, which have simple geometric shapes. Then these elements are expressed using some unknown values at specific positions in the elements, with some assumptions about the points and the governing relationships. These specific points are called nodes. Apply the boundary conditions to these elements to connect them again, a set of algebraic equations are acquired[11]. These equations can be expressed in this form:

$$[K]\{u\} = \{F\} \tag{6}$$

where *[K]* is the property, *{F}* is the action, and *{u}* is the behaviour.

In these three parameters, *{u}* is the unknowns one that should be solved. Thus, the above equation can be rewritten like this:

$$\{u\} = [K]^{-1}\{F\} \tag{7}$$

Solutions of these equations tell the engineers the approximate behaviour of this system[7]. These solutions can be used later for further calculations. For these approximate solutions, error analysis is necessary.

Hence, the various steps of FEM are[8]:

(1) Select suitable field variables and the elements,
(2) Discritize the system,
(3) Select proper nodes (select interpolation functions),
(4) Find the properties of element,
(5) Put element properties together to obtain the global properties,
(6) Apply the boundary conditions,
(7) Solve the system equations to get the unknown values,
(8) Make the additional calculations to get the required values, and
(9) Error analysis.

Compared with other EEG source localization projects, this project did not select the simple spherical model to represent the head geometry but used the realistic model. This made the problem more complex and it is difficult to solve this problem. Therefore, FEM was introduced in this project.

Following the steps of FEM given above, the potential values at specific positions on the scalp were the required variables. Those positions are the points where the EEG electrodes were put. In order to measure those potentials, the 2D/3D head model was divided into many meshes first. The size of each mesh is 1mm×1mm/1mm×1mm×1mm.

2.3 Inverse Problem

EEG inverse problem uses the scalp EEG signal to estimate the corresponding current source inside the brain. It is an ill-posed problem, i.e., an underdetermined problem and no unique solution can be given[12]. The reasons for these issues are the space of possible source distribution has infinite dimension and the number of electrodes is finite.

Different inverse approaches can be classified into two groups, non-parametric method and parametric method. The non-parametric method works on the distributed source model where the number of dipoles is unknown but the locations and orientations are fixed. Parametric method, on the other hand, needs fewer dipoles and the number of dipoles is fixed. Compared with the non-parametric method, parametric method can estimate the current dipole nicely. Therefore, the parametric method was applied to solve the EEG inverse problem in this project.

In order to get unique result, the location and the moment of the current dipole was given in this project. Also, the least squares sense was used and a minimization problem was solved to obtain the estimated source position.

There are three main steps in this project. Firstly, initiate the dipole at a proper position in the reference model and calculate the corresponding scalp potentials. Then calculate the potentials of each grey matter point in the modelling group. Both the steps are forward problem in a way. Comparing all sets of potentials in the modelling group with the potentials of reference model, one set of data in the modelling group that has the smallest difference is selected and the corresponding position in the grey matter is termed as estimated dipole. This step is inverse problem.

According to (5), the EEG forward problem is to solve the Poisson's equation to find the scalp potentials V. This parameter is determined by three factors, the electrode position r, the dipole position r_{dip} and the dipole moment e_d. For one dipole and one electrode, the electrode potential is:

$$u(r) = g(r, r_{dip}, e_d) \tag{8}$$

In this equation, $g(r, r_{dip}, e_d)$ indicates the potential at an electrode positioned at a point on the scalp with position vector r generated by a single dipole with dipole moment e_d located at r_{dip} inside the brain.

Assume the superposition principle, another form of (8) could be given, which is:

$$u(r) = g(r, r_{dip})e_d \tag{9}$$

If the number of electrodes is extended to N, (9) can be re-written in the following way:

$$U = \begin{bmatrix} u(r_1) \\ u(r_2) \\ \vdots \\ u(r_N) \end{bmatrix} = \begin{bmatrix} g(r_1, r_{dip}) \\ g(r_2, r_{dip}) \\ \vdots \\ g(r_N, r_{dip}) \end{bmatrix} e_d = GM \tag{10}$$

where G is called gain matrix, each row of which gives the current flow for the specific electrode[12], and M is the dipole moment matrix.

According to (10), both the scalp potentials of the dipole in the reference model U_{meas} and the potentials of each grey matter point in the modelling group U_{cal} can be received

For the comparison work, the least squares sense was applied, which is:

$$d^i = \lVert U_{meas} - U_{cal}^i \rVert = \sqrt{\sum_{j=1}^{N} \left[U_{meas}(j) - U_{cal}^i(j) \right]^2} \tag{11}$$

where i is the index of the grey matter points vector.

The set of U_{cal} which gave the smallest d was generated by the position where the estimated dipole should be placed. Thus, the minimization problem should be solved, which is:

$$D = min \lVert U_{meas} - U_{cal}(r_g) \rVert \tag{12}$$

where r_g is the position which is considered as the estimated source position.

To evaluate the results, three parameters were calculated, which are localization error (LE), relative error (RE) of the potentials and the orientation error (OE). The localization error is the distance between the estimated source position and the actual dipole position. It is defined as:

$$LE = \lVert Dipole\ position - Estimated\ position \rVert \tag{13}$$

The relative error is defined as:

$$RE = \frac{\sqrt{\sum_{e=1}^{N}(V_{cal}^{e} - V_{meas}^{e})^{2}}}{\sqrt{\sum_{e=1}^{N}(V_{meas}^{e})^{2}}} \tag{14}$$

where e is the index of the electrode vector, V_{meas} is the potentials of the actual dipole, and V_{cal} is the potentials of the estimated source. The orientation error is defined as:

$$OE = \cos^{-1}\left(\frac{\boldsymbol{M}_{dipole} \cdot \boldsymbol{M}_{est}}{\|\boldsymbol{M}_{dipole}\|\|\boldsymbol{M}_{est}\|}\right) \tag{15}$$

where $\boldsymbol{M}_{dipole}$ is the actual dipole moment and $\boldsymbol{M}_{est}$ is the estimated source moment.

CHAPTER 3 CHALLENGES AND LIMITATIONS

In EEG source localization, there are some challenges and limitations that restrict the result accuracy. These challenges and limitations could be caused by different factors. This chapter will discuss these issues.

Inaccurate Conductivity Values

The EEG source localization is a method relying on electrical tissue conductivities[13]. Accurate conductivity values can improve the accuracy of the head model and give better estimation. However, it is a big problem to determine most of the tissues' conductivity values. The ideal condition is to use the in vivo conductivity values, but it is impossible to measure these values in living patient without surgery[14]. Thus, some assumptions are needed. Unfortunately, due to the high inhomogeneity and even anisotropy of the tissue conductivities[15], even the assumptions are hard to make. If some lesions exist inside the brain, the problem becomes even more complex. As the lesion's conductivity value is totally different from the normal tissues surrounding them, eccentric conductive inhomogeneity in the head volume conductor is generated[14]. Because of the above reasons, there exists a big challenge in EEG source localization.

Intensity Inhomogeneity

Magnetic Resonance Imaging (MRI) is used in EEG source localization due to its several advantages compared with other diagnostic imaging techniques. It has high spatial resolution, which makes this technique sensitive to the subtle structure changes or abnormities. It can describe the soft tissues perfectly, especially for clinical diagnosis of cerebral and cardiac diagnose. More important, it is not hazardous for patients. For many years, 1.5T is the gold standard magnetic flux density in MR systems. Currently, the high field MRI has been applied, which gives higher signal-to-noise ratio (SNR) and shorter acquisition time. However, high field MRI also has some defects. The main problem is that the high field MRI introduces RF inhomogeneity. This problem leads to the intensity inhomogeneity: the pixels of the same tissue may have totally different intensity values while the pixels belonging to different tissues may have the similar intensities[16]. This means that in the intensity histogram, each tissue covers large area and there could be big overlapping between two tissues. The overlapping causes big challenge when doing tissue segmentation: Tissues cannot be segmented perfectly. As a result, the estimation accuracy will be affected.

Software Limitation

There are several software packages that can be used in brain tissue segmentation, such

as SPM, FreeSurfer, FSL, and etc. In this EEG source localization project, FMRIB Software Library (FSL) is utilized to segment the MR images. This is a comprehensive, self-contained package for MRI data analysis. It has some advantages compared with other segmentation software packages. According to[17], FSL can segment more tissues than SPM and give better segmentation results than FreeSurfer. However, the limitation of this software cannot be ignored. Maximally, it can only segment five tissues efficiently: Scalp, skull, white matter, grey matter and CSF. It is possible to segment more tissues, but the errors will be very high.

CSF Segmentation

Cerebrospinal fluid (CSF) is produced by the choroid plexus in the ventricles (cavities within the brain). It occupies the subarachnoid space constructed by the arachnoid mater (the middle layer of the brain cover) and the pia mater (the innermost layer of the membranes covering the brain). Because the brain and the CSF are similar in density, the brain can float in and be protected by CSF. This means that CSF spreads widely inside the brain, either around the skull or surrounding the grey matter and other tissues.

Figure 3.1 The distributions of grey matter, white matter and CSF

This wide distribution brings problem when CSF should be segmented. The analysis described in[17] showed that FSL performed erroneous CSF segmentation. There are other software that can do better CSF segmentation, e.g. SPM. However, as FSL was used in this EEG source localization project, CSF segmentation could be a big challenge for getting good estimated source position.

CHAPTER 4 METHODOLOGY

This chapter describes different methods applied in this research work and the way it was carried out. In this project work, the modified subtraction method[18] is used to model the dipole for forward problem. The inverse problem in EEG source localization uses the scalp EEG signal to estimate the corresponding current source inside the brain and it is an ill-posed problem. To attain uniqueness it is necessary to impose a priori knowledge on the source distribution. For the inverse problem, the common practice is followed and the parameters that give the best fit in least squares sense are chosen. An exhaustive search pattern, i.e., inversion was performed for each possible source location in the cortex area inside the brain, and the location producing the smallest residual norm was selected as the best possible source location.

There are two data sources applied in this project, the virtual family database and the real MR images. Depending on the materials used for simulation, the whole project was mainly divided into two phases: model studies and noise effects using virtual family data in 2D and segmentation effect studies using real MR images in 3D. The segmentation was performed using FSL.

4.1 Tissue Model Study and Noise Effect Study

In this section, the performance of different tissue models was assessed, i.e. different models were generated with different combinations of the tissues. Then signal noise and conductivity noise were introduced separately to understand how they effect and influence the source localization. The general procedures are:

Step 1: Use all the available tissues to build the reference model and calculate the potentials of the fixed dipole. These potentials are used as the reference EEG signal.

In case of the signal noise study, the noise will be added to the reference EEG signal.

Step 2: Construct different head models using different tissue components. In each head model, calculate the potentials of all grey matter points.

In case of the conductivity noise study, the noise is added to the head model that performs the best in tissue model study.

Step 3: Calculate the goal function between the potentials of each grey matter point in the estimated head model and the potentials of the actual dipole according to (11). Exhaustive search was performed in this step in order to find all the grey matter points.

Step 4: Normalize the goal function values of each grey matter point and find the minimum value in these normalized values.

Step 5: Find the estimated dipole position and check the localization, error relative error and the orientation error between the estimated source and the actual dipole using (13), (14) and (15).

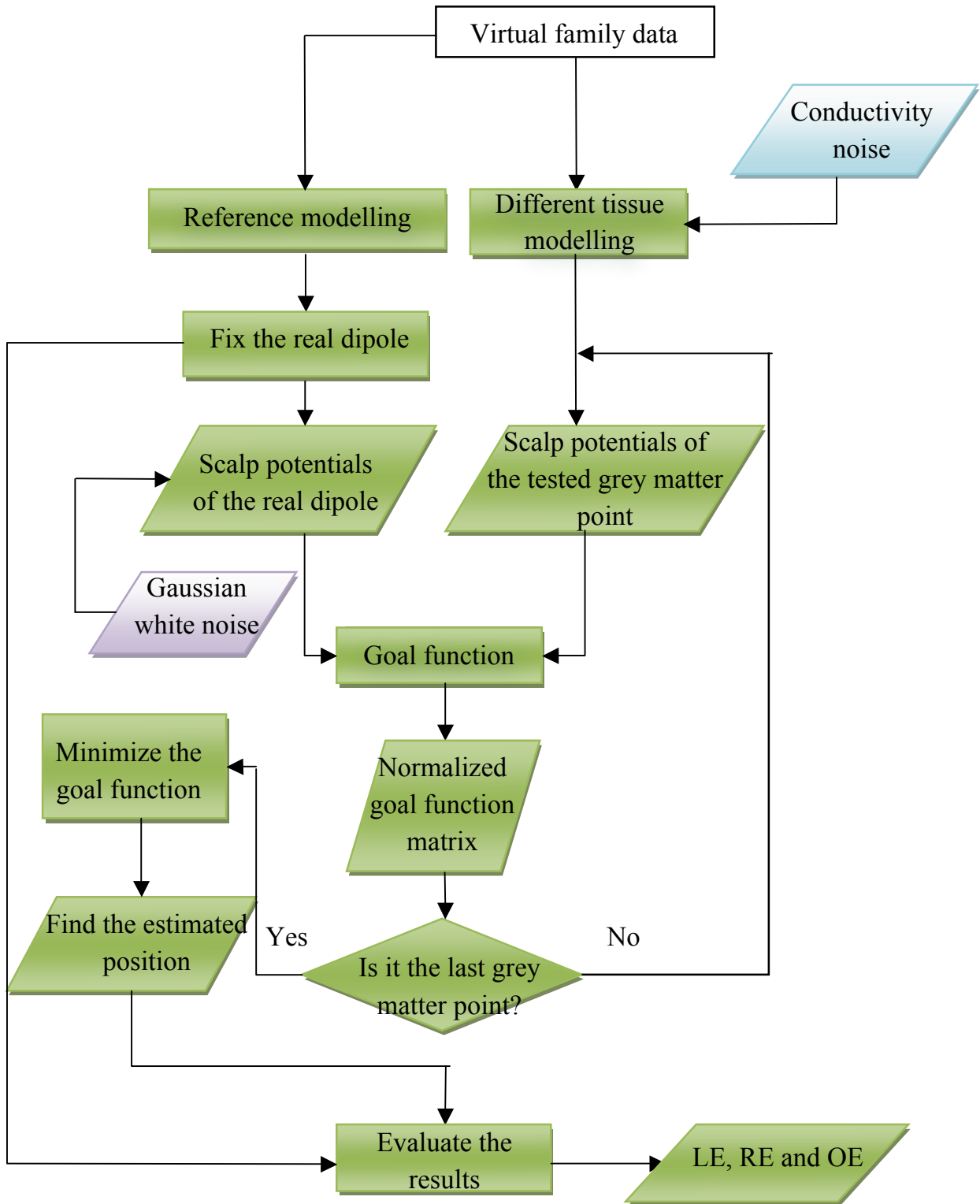The above algorithm is shown in the form of a flowchart below:

Figure 4.1 Work frame of simulation using virtual family

4.1.1 Different tissue models

The existence of the significant tissues was verified before starting the study. The virtual family model utilized in this project contains 10 tissues: scalp, marrow red, fat, skull, grey matter, connective tissue, blood vessels, white matter, cerebellum and cerebral spinal fluid (CSF). The conductivity values were taken from a database[19]. The conductivities of tissues of less significance were changed to the important tissues with respect to the structural proximity. This study was simulated to understand the effects of head-model complexity on the EEG source localization and find out the optimal number of tissues for the head-model. Six head models with number of tissue vary from 4 to 9 were compared with a reference head model, i.e., a model with all available tissues. The model configuration is given below:

Model 0: This head model consists of all ten tissues, which are listed in Table 1 and this head model is considered as the reference model (Model ref).

Model 1: This head model is derived from Model 0 in which the conductivity of grey matter is set equal to the white matter, i.e. a nine tissue-type head model.

Model 2: This head model is derived from Model 0 and the conductivities of grey matter and CSF are set equal to the white matter, i.e. an eight tissue-type head model.

Model 3: This head model consists of scalp, skull, white matter, grey matter and CSF, i.e. a five tissue-type head model. This head model is also derived from Model 1 by replacing other tissue's conductivity values with the adjacent tissue's values.

Model 4: This head model is derived from Model 3 where the conductivity of CSF is given the grey matter's value, i.e. a four tissue-type head model.

Model 5: This head model is also derived from Model 3 and it is a four tissue-type head model. In this head model, the CSF is set the same as the white matter.

Model 6: This head model is derived from Model 3 but with conductivity of CSF equal to the bone, i.e. a four tissue-type head model.

Table 4-1 shows the relative percentage of occupancy of each tissue, tissue availabilities and conductivity values in each model. In this table, the letter "Y" means that the corresponding tissue is available on the model and "N" means the tissue is not available on the model. A reference head model was used to create synthetic EEG signals by placing the artificial source inside the model to mimic the clinical data from patients. For the inverse source localizations an exhaustive search method was used to estimate the best dipole position and orientation with the synthetic EEG data thus all the possible positions were

searched in the cortex. The estimated mean localization errors were the best results one could localize from a given model.

Table 4-1: Head tissue percentage, tissue availabilities and conductivity values in each model

Tissues	Percent (%)	Ref. Model Value	Ref. Model Y/N	Model 1 Value	Model 1 Y/N	Model 2 Value	Model 2 Y/N	Model 3 Value	Model 3 Y/N	Model 4 Value	Model 4 Y/N	Model 5 Vlaue	Model 5 Y/N	Model 6 Value	Model 6 Y/N
GM	38.3	0.089	Y	0.058	N	0.058	N	0.089	Y	0.089	Y	0.089	Y	0.089	Y
WM	21.9	0.058	Y	0.058	Y	0.058	Y	0.058	Y	0.058	Y	0.058	Y	0.058	Y
CSF	13.4	2.000	Y	2.000	Y	0.058	N	2.000	Y	0.089	N	0.058	N	0.020	N
Fat	6.4	0.021	Y	0.021	Y	0.021	Y	0.020	N	0.020	N	0.020	N	0.020	N
Marrow red	2.5	0.002	Y	0.002	Y	0.002	Y	0.020	N	0.020	N	0.020	N	0.020	N
Skin	5.9	0.000	Y	0.000	Y	0.000	Y	0.000	Y	0.000	Y	0.000	Y	0.000	Y
Skull	8.9	0.020	Y	0.020	Y	0.020	Y	0.020	Y	0.020	Y	0.020	Y	0.020	Y
Connective tissue	1.7	0.163	Y	0.163	Y	0.163	Y	0.089	N	0.089	N	0.089	N	0.089	N
Cerebellum	0.8	0.109	Y	0.109	Y	0.109	Y	0.089	N	0.089	N	0.089	N	0.089	N
Blood vessels	0.3	0.7	Y	0.7	Y	0.7	Y	2.000	N	0.089	N	0.058	N	0.058	N

Compared with the first three models (Model 1, Model 2 and Model 3), Model 4, Model 5 and Model 6 replaced the CSF with the tissues that exist around CSF in the brain. In practice, it is common that the conductivity value of CSF can be replaced by the conductivity values of adjacent tissues. Therefore, it is necessary to consider this condition.

In this 2-D study, all the head models have the mesh resolution of 1×1 mm. All the models had 14,078 cells and 16,004 nodes. 30 electrodes were placed around the model and the distances between each two adjacent electrodes are equal. The forward problem was solved for both the actual dipole in the reference head model and each grey matter point in all other head models. The dipole was set to be y oriented dipole and the x and y coordinates of

this dipole were 0.0470 and 0.0550 and the dipole moment was (0.0000, 0.1000). Figure 4.2 shows the reference head model, the actual dipole position and the dipole moment.
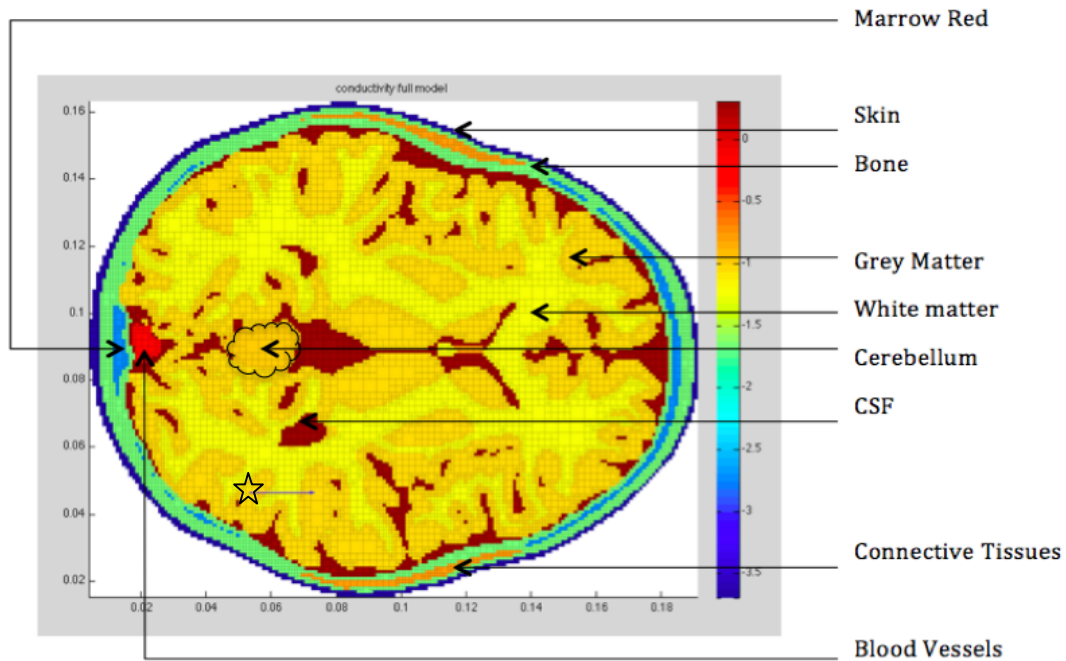

Figure 4.2 The reference head model and the actual dipole. The star shows the dipole position and the blue arrow gives the moment of this dipole.

4.1.2 Signal noise study

A more realistic case closer to the clinical practice is to add noise to the model. In practice, noise exists everywhere. There are aberrations and disturbances in the signal obtained from the scalp using the electrodes. Therefore, in this EEG source localization project, the random Gaussian white noise was added to achieve the desired signal to noise ratio (SNR). In the real EEG, SNR usually has a value between 6 to 10 where the SNR is defined as:

$$SNR = 10 \log \left(\frac{P_{signal}}{P_{noise}} \right) \qquad (16)$$

where P_{signal} is the power of the signal, and P_{noise} is the power of the noise. The additive noise was generated such that its power spectrum matches the power spectrum of human EEG[6]. As a result, the influence caused by noise could be studied. For each value of SNR, it was repeated for 200 times.

To analyze the results, the standard derivations (*STD*) for all the SNR values in all the

head models were calculated. This is the parameter that describes the dispersion of a set of data from the average. Low standard derivation value means that all data points are close to the mean value. Standard derivation is the square root of variance and can be defined as:

$$STD = \sqrt{\frac{1}{N}\sum_{i=1}^{N}(x_i - \bar{x})^2} \tag{17}$$

where x_i is the *ith* point in this data set and $\bar{x}$ is the average value of the data set.

4.1.3 Conductivity noise study

Conductivity noise is also called conductivity uncertainty. There are two main reasons for the occurrence of this problem. Firstly, it is impossible to measure the actual conductivity values in a living body. Another reason is that little attention is paid to brain lesion, which could create dramatic effect from normal tissues[14]. In this part of study, the influence of the conductivity noise was analyzed and the acceptable range of noise was obtained.

In this study, a random Gaussian noise with δ was added to the tissue conductivity values according to the following formula:

$$\sigma_{new} = \sigma + \delta \times rand \tag{18}$$

where σ_{new} is the new conductivity values after adding conductivity noise, σ is the original conductivity values, δ is the variance values, *rand()* is a random Gaussian noise with zero mean and variance one. 15 variances were applied in this study. Those seven values are 0.005, 0.01, 0.015, 0.02, 0.025, 0.03, 0.035, 0.04, 0.045, 0.05, 0.06, 0.07, 0.08, 0.09 and 0.1. For each variance, the same procedure was repeated for 200 times.

4.2 Segmentation Tools

FSL can be defined as an integrated library with the analysis tools for functional magnetic resonance imaging (fMRI), diffusion tensor imaging (DTI) and MRI brain image data. It is developed by the functional MRI of the brain (FMRIB) analysis group at the Oxford Centre in United Kingdom (UK)[20, 21].

The tools available in FSL can be used to segment the brain into its constituent tissues; it can also be used to extract only the brain and also to register two images. There are many other tools used with respect to the need. The tools are available separately for functional

MRI data, structural MRI data and diffusion MRI data. This section is about the structural MRI tool used in the project and the way it helps in obtaining structural importance of the anatomical structures in order to compare them.

The main concern in any medical imaging application is the accurate brain segmentation. Also, the brain must be segmented into its constituent parts from the non-brain tissues. FSL implement brain segmentation by doing the following steps: Firstly, the input image should be registered with the reference image using *FMRIB's Linear Image Registration Tool (FLIRT)*; Secondly, *Brain Extraction Tool (BET)* is applies to extract scalp and skull from the registered image; Then the brain is segmented into grey matter, white matter and CSF using the function called *FAST*, which is the abbreviation of *FMRIB's Automated Segmentation Tool*. Finally, five tissues were given as the outputs, which are scalp, skull, white matter, grey matter and CSF[20].

In order to get rid of the motion artefacts, a tool called MCFLIRT is also used. MCFLIRT and FLIRT use the same technique.

4.3 Segmentation effect studies

This section discusses the effects of segmentation on the source localization. Segmentation in medical imaging is one of the most critical and important concepts. In order to realize and get the realistic analysis, the brain has to be segmented into its constituent parts correctly. The most accurate segmentation gives the most realistic head model.

In this project, FSL, the most common used segmentation software, was utilized to segment the 3D MR images. Giving different threshold values and by applying BET, three different models were generated by extracting the skull from the image generated. This threshold determines the amount of skull extracted from the MR image. The smaller this value is, the larger the brain's outline is estimated. The threshold values used were 0.3, 0.4 and 0.5.

When the segmentation process was performed, the Dice's coefficient was calculated. This coefficient is a similarity coefficient indicating the agreement between two data sets[22, 23]. The definition of the Dice's coefficient is given below. Assume i_1 and i_2 are two individuals. Each of them has a binary vector, which describe the distribution of the data. For these binary vectors, 1 designates presence and 0 designates absence of a sample at some position. Denoting a = the number of positions shared by both individuals, b = the number of positions occupied only by i_1, c = the number of positions taken only by i_2[23], d = the number of positions belonging to none of these two individuals, and n = the total number of the two individuals, that is $n = a+b+c+d$. Then the Dice's coefficient is given in the following

formula[23]:

$$D(i_1, i_2) = \frac{2a}{2a + b + c} \tag{19}$$

In this project, one of the individuals is the ground truth and the other is the estimated model. Table 4-2 to Table 4-4 show the Dice's coefficients for the three models in this project.

Table 4-2: Dice's coefficients for model with threshold = 0.3

	White Matter	Grey Matter	CSF	Skull	Inner Skin	Outer Skin
White Matter	629919	44502	0	0	265	2
Grey Matter	13324	801639	84082	0	0	257
CSF	0	69156	301166	0	0	1623
Skull	0	0	3493	358602	0	466
Inner Skin	0	0	12222	39433	674679	315
Outer Skin	45	0	0	0	0	4045428

Table 4-3: Dice's coefficients for model with threshold = 0.4

	White Matter	Grey Matter	CSF	Skull	Inner Skin	Outer Skin
White Matter	630565	44212	0	0	0	0
Grey Matter	9646	790751	102515	0	0	0
CSF	0	62	371883	0	0	0
Skull	0	0	3959	358602	0	0
Inner Skin	0	0	12537	0	714112	0
Outer Skin	12	0	0	0	0	4055395

Table 4-4: Dice's coefficients for model with threshold = 0.5

	White Matter	Grey Matter	CSF	Skull	Inner Skin	Outer Skin
White Matter	630471	44247	0	0	23	23
Grey Matter	10527	788226	102184	0	0	1178
CSF	0	6908	357544	0	0	7493
Skull	0	0	3046	357855	0	913
Inner Skin	0	0	11002	1516	712596	1535
Outer Skin	12	0	0	0	0	4054877

The source localization was done using these three models in MATLAB. The procedures are the same as the simulations using virtual family data in 2D. The coordinates of the initial dipole's position are 0.1125, 0.1100 and 0.1020.

CHAPTER 5 RESULTS

5.1 Model study

To check the performance of different head models, the potentials generated by the same dipole in different head models and the goal function of each head model are given. Figure 5.1a shows scalp potentials of the real dipole in the reference model and Figure 5.1b shows goal functions in the reference model.
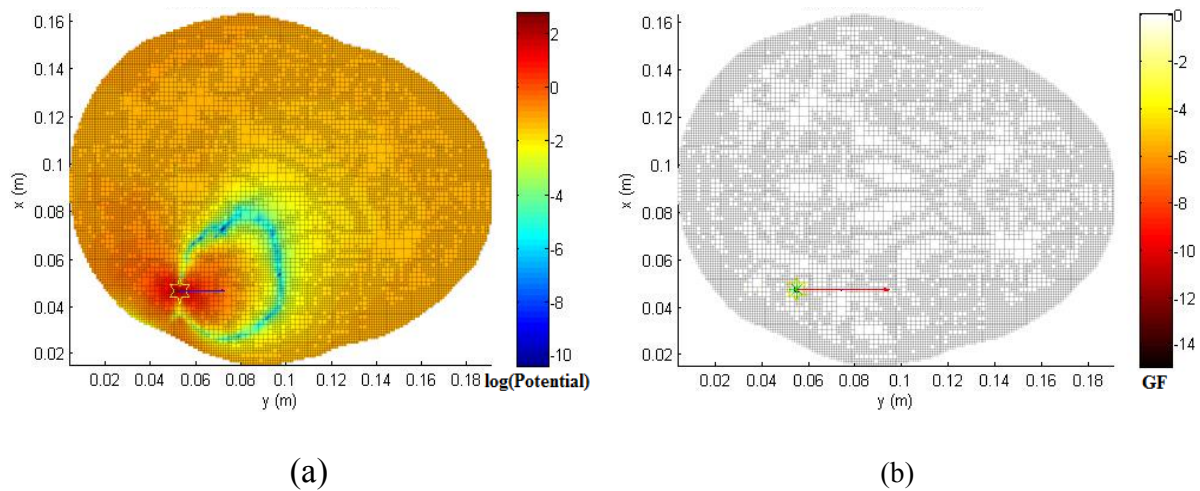

<div style="text-align:center">(a)   (b)</div>

Figure 5.1 (a) Potentials inside reference model and (b) the goal functions of reference model. The yellow star shows the position of the actual dipole and the blue arrow shows the moment of this actual dipole. The green point shows the estimated source position and the red arrow shows the moment of the estimated dipole.

The patch plot of scalp potentials of a *Y*-oriented dipole of six tested head models are shown in Figure 5.2. Compared with the potentials generated in the reference model, the potentials generated by Model 3 are closest to the reference potentials. Model 2, Model 4, Model 5 and Model 6 give the potentials that are very different from the reference potentials. Also, the Model 1 with 9 tissues, have error more than the Model 3 with 5 tissues. To get better understanding, Table 5-1 was given. This table shows the relative error between the potentials generated by the actual dipole in the reference model and the potentials generated by the same dipole but in the reconstructed head model. Both the table and the figures show that Model 3 performed the best. This means that the number of tissues used to build the head model is not immaterial. But, the type of the tissues is the key factor.
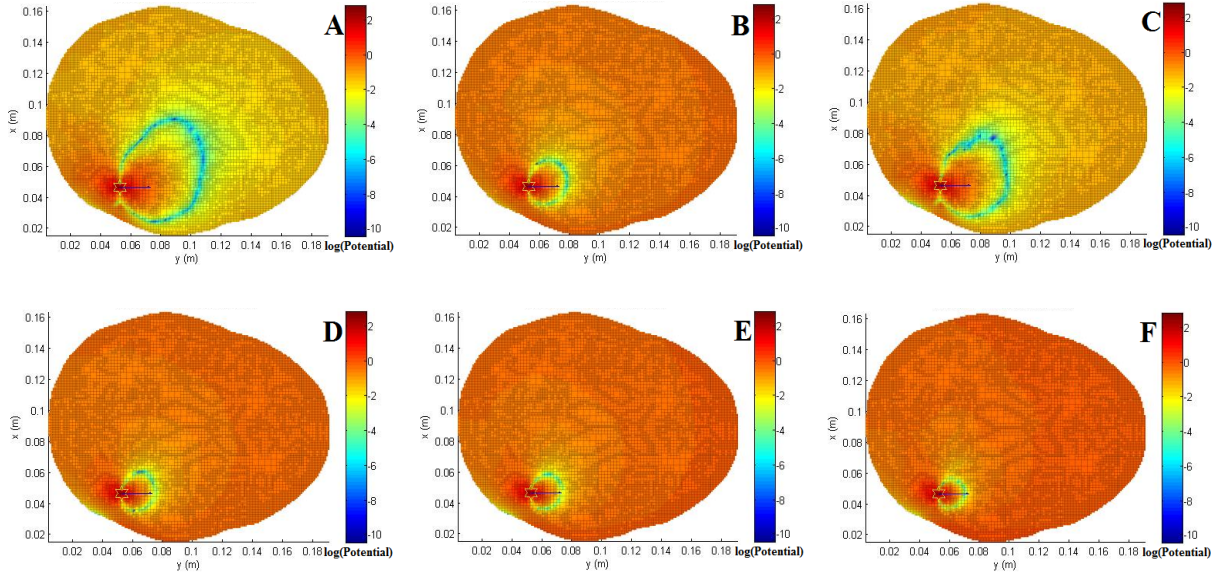
Figure 5.2 Scalp potentials of six head models for an x oriented dipole in patch plot. (A) Model 1 with nine tissue-types. (B) Model 2 with eight tissue-types. (C) Model 3 with five tissue-types. (D) Model 4 with four tissue-types. CSF is given grey matter's conductivity value. (E) Model 5 with four tissue-types. CSF is given white matter's value. (F) Model 6 with four tissue-types. CSF is given bone's value. The potentials are given in logarithmic format. The star shows the position of the actual dipole and the arrow shows the moment of the actual dipole.

Table 5-1: Relative errors between the reference model potentials and the reconstructed model potentials of the actual dipole (RE$_{same}$)

	Model 1	Model 2	Model 3	Model 4	Model 5	Model 6
RE$_{same}$ (%)	38.03	61.40	0.34	24.77	28.31	36.78

Figure 5.3 is the goal functions of different estimated models. The goal function gives the relative error between the potentials at scalp due to real dipole and potentials at scalp due to each grey matter's scalp potentials in each model. In order to get better visulization, the logarithmic scale is chosen in the figures. In Figure 5.3, white meshes belong to the non-grey matter tissue types. Those meshes were not considered during exhaustive search; Colour meshes are meshes that belong to grey matter. The darker the colour is the smaller relative error this mesh has, and the darkest place is the position where the estimated dipole should be located. Compare each model's goal functions with the goal functions shown in Figure 5.1b and consider about the real dipole's position as well, it is found that Model 3 works the best. The position estimated by using Model 3 is almost the same as the real dipole's position.

Model 2, Model 4, Model 5 and Model 6 gave the bad results. Areas with minimum relative errors are far from the reference dipole position compared with Model 1 and Model 3. All these models had CSF merged with some other tissue. This indicates that CSF plays a vital role in EEG source localization method.
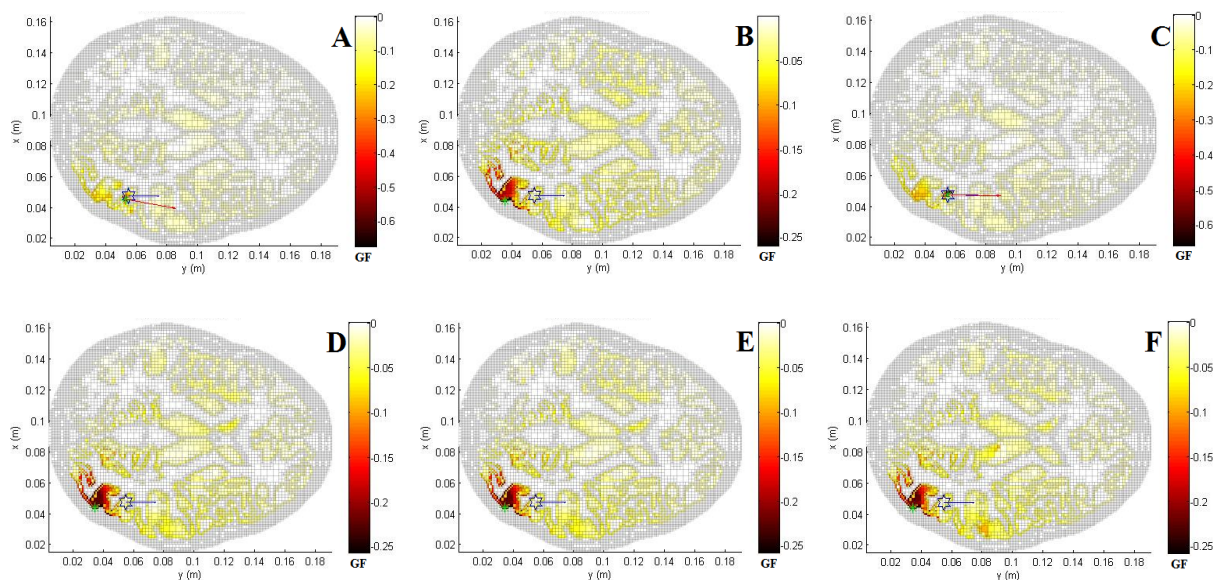

Figure 5.3 Goal functions of different head models. (A) Goal functions for Model 1 with nine tissue-types. (B) Goal functions for Model 2 with eight tissue-types. (C) Goal functions for Model 3 with five tissue-types. (D) Goal functions for Model 4 with four tissue-types. CSF is given grey matter's conductivity value. (E) Goal functions for Model 5 with four tissue-types. CSF is given white matter's value. (F) Goal functions for Model 6 with four tissue-types. CSF is given bone's value. The blue star indicates the actual dipole's position and the blue arrow indicates the actual dipole's moment. The green point indicates the estimated dipole's position and the red line is the estimated dipole's moment.

Table 5-2 lists the estimated dipole positions in all models. The localization errors (LE), orientation errors (OE) and the relative (RE) for different models are also represented in this table. The relative errors in this table are the one between potentials of the actual dipole and potentials of the estimated source (RE_{diff}).

Table 5-2: Estimated positions and errors of different head models

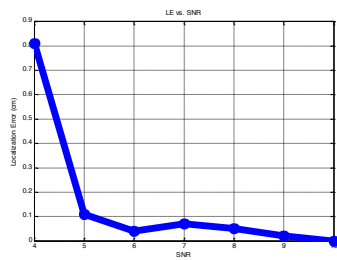| Models	Estimated Positions	LE (cm)	Estimated Moments	OE (deg)	RE$_{diff}$ (%)
Reference	(0.0470, 0.0550)	0	(0.0000, 0.1000)	0	0
Model 1	(0.0450, 0.0530)	0.28	(-0.0148, 0.0813)	0.1796	21.13
Model 2	(0.0435, 0.0355)	1.98	(-0.0000, -0.0000)	3.0568	54.97
Model 3	(0.0470, 0.0550)	0	(-0.0010, 0.0859)	0.0111	21.91
Model 4	(0.0435, 0.0345)	2.08	(-0.0000, -0.0000)	3.0453	55.30
Model 5	(0.0435, 0.0345)	2.08	(-0.0000, -0.0000)	3.0432	55.20
Model 6	(0.0435, 0.0345)	2.08	(-0.0000, -0.0000)	3.0384	55.11

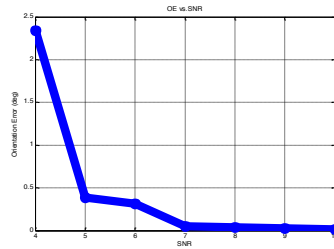## 5.2 Noise effects

5.2.1 Signal noise

Based on the model study's results, Model 3 was used for the noise study part. In real EEG the background signals have frequency between 8 to 13Hz, known as Alpha rhythm, and its amplitude is in the range 30 to 40 µV. The spike signals usually have duration in the range 30 to 70ms. The amplitude of these signals could be from 100 to 200 µV. Noises with different levels of SNR were added to the reference EEG signals. Table 5-3 lists the results for different noise levels. Figure 5.6 shows results for EEG signals contaminated with noises. As shown in Figure 5.6a the EEG source localization results have LE less than 1mm, which is the model resolution for SNR 6 and higher. Figure 5.6b shows the orientation results and Figure5.6c shows the standard derivation results. Both the table and the figure show that, with the increasing of SNR values, the errors will decrease.

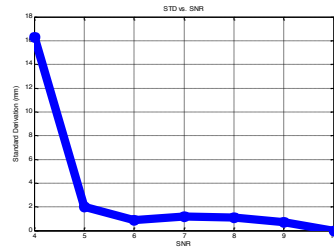**Table 5-3 Numerical analysis of the signal noise study**

SNR	LE (cm)	OE (deg)	RE$_{diff}$ (%)	STD (mm)
4	0.81	2.3390	85.4	16.3
5	0.11	0.3865	81.85	2
6	0.04	0.3152	72.35	0.9
7	0.07	0.0515	63.21	1.2
8	0.05	0.0416	45.49	1.1
9	0.02	0.0263	33.2	0.7
10	0	0.0152	27.41	0

(a)   (b)   (c)

Figure 5.6 (a) LE, (b) OE and (c) STD for Model 3 with added noise to the EEG signals.

5.2.2 Conductivity noise

Figure 5.7a shows the Model 3 with no conductivity noise and Figure 5.7b shows the reference EEG of the actual dipole. The noise is added randomly to the variance to generate the new conductivity values. In order to get good statistical results, for each variance value, the same procedure is repeated 200 times so that the average value gives the optimum result.
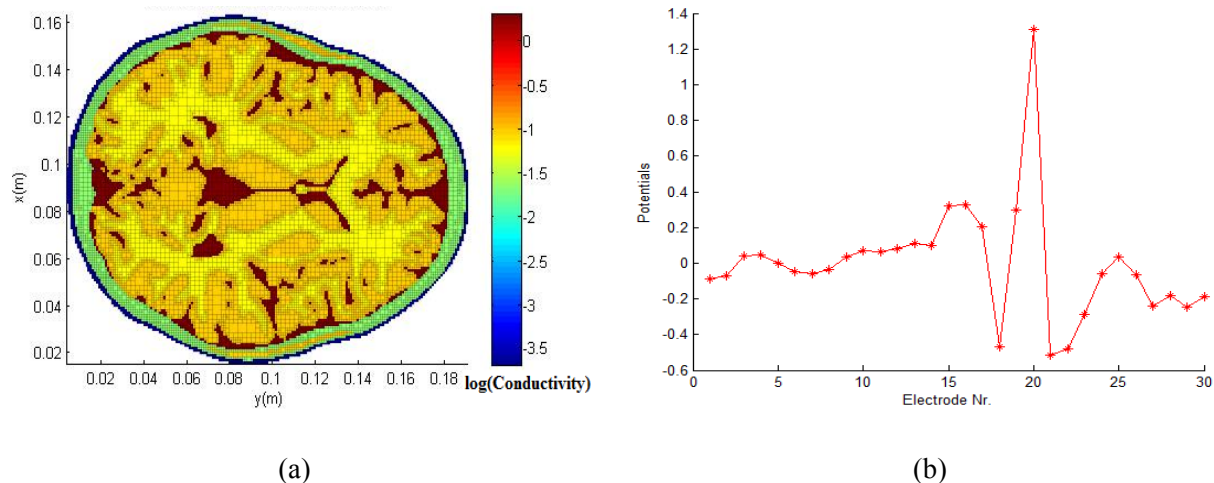
(a)   (b)

Figure 5.7 (a) Model 3 with no conductivity noise (variance = 0) and (b) the reference EEG from the actual dipole in Model 3 with no conductivity noise. In Figure (b), the *x* axis is the index of the electrodes.

Figure 5.8 and Figure 5.9 show the EEG differences. Figure 5.8 is the potentials of the same dipole (reference dipole) but generated in different conductivity noise conditions. Figure 5.9 shows the potential differences between the potentials generated by the reference dipole and the potentials generated by the estimated dipole in different conductivity noise conditions. Table 5-4 shows the numerical analysis results.

Figure 5.8 shows that EEG source localization problem is not sensitive to conductivity noise. With the increasing of variance values, the differences of potentials generated by the reference dipole and the reference potentials are not very big until the variance equals to 0.07. However, the accuracy became very poor when the variance value is higher than 0.02. The potentials generated by the reference dipole and the potentials generated by the estimated dipole had significant differences even when the variance is higher than 0.01. This can be seen from Figure 5.9 and Table 5-4. Figure 5.9 also shows that different positions could generate similar or even the same EEG signals. Potentials generated by the third estimated dipole (Figure 5.9c) and potentials generated by the forth estimated dipole (Figure 5.9d) are almost the same, and potentials generated by the seventh estimated dipole and potentials generated by the ninth estimated dipole are very similar. Figure 5.10 shows results for conductivity noise study. As shown in Figure 5.10a the EEG source localization results have LE less than 1cm, which is the conductivity noise less than 0.02. Figure 5.6b shows the relative errors between the potentials generated by the reference dipole and the potentials generated by the estimated dipole and Figure5.6c shows the standard derivation results. Both the table and the figure show that, with the increasing of variance values, the errors will increase as well.
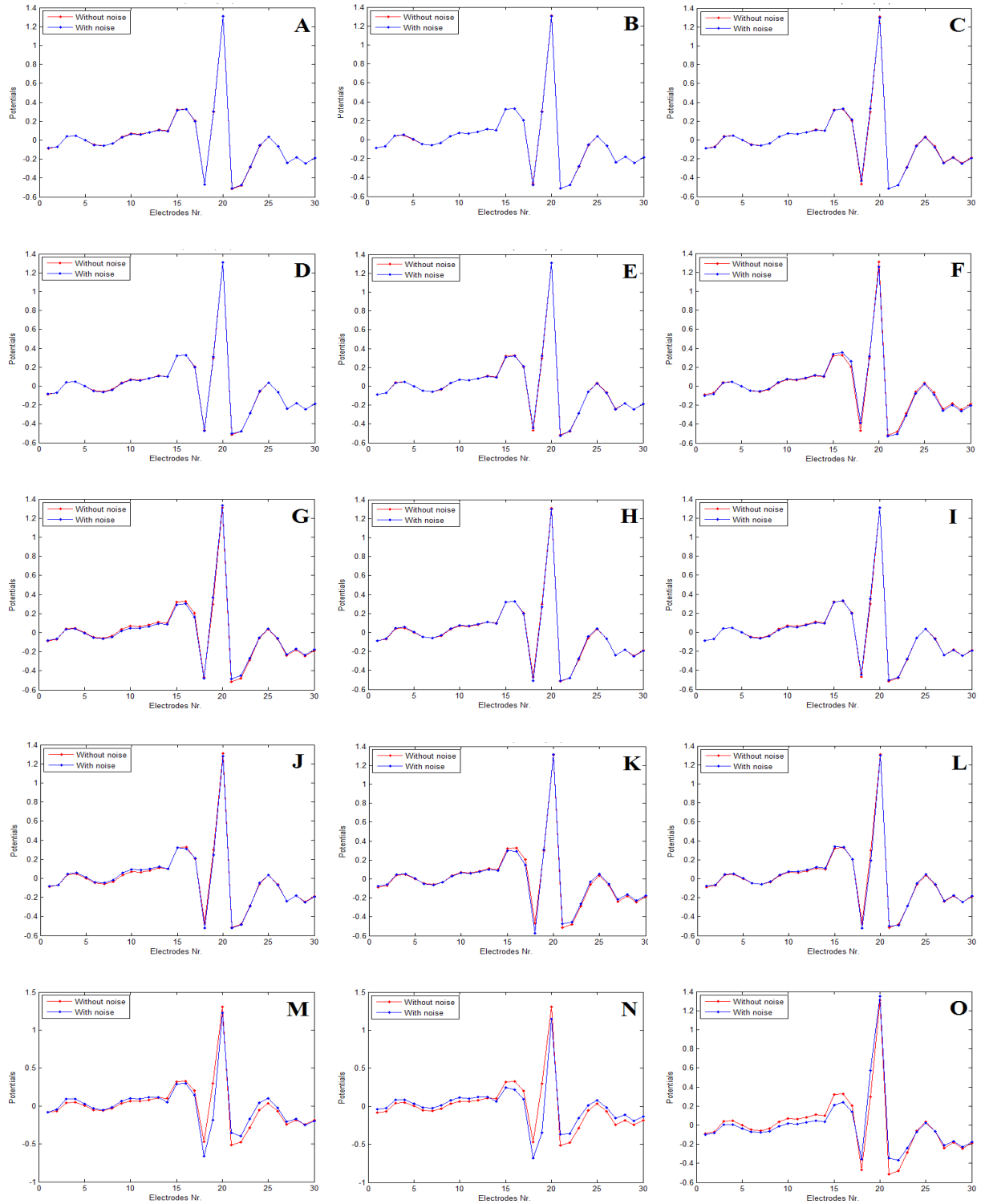
Figure 5.8 EEG of the reference dipole of Model 3 with different conductivity noises (variance, Var.). (A) Var. = 0.005. (B) Var. = 0.01. (C) Var. = 0.015. (D) Var. = 0.02. (E) Var. = 0.025. (F) Var. = 0.03. (G) Var. = 0.035 (H) Var. = 0.04 (I) Var. = 0.045 (J) Var. = 0.05 (K) Var. = 0.06 (L) Var. = 0.07 (M) Var. = 0.08 (N) Var. = 0.09 (O) Var. = 0.1. Red curve is the reference dipole EEG and the blue one is the estimated dipole EEG.
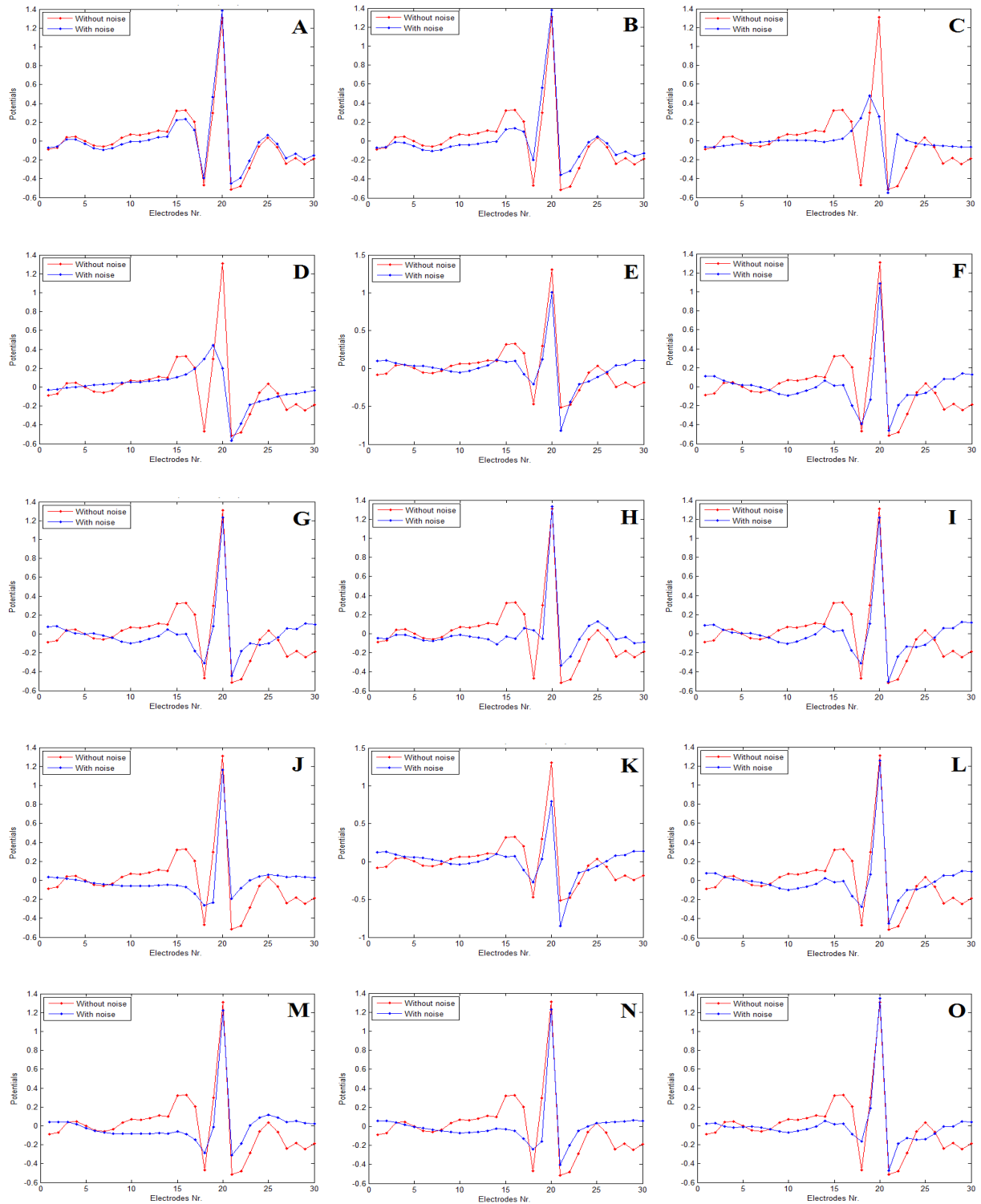
Figure 5.9 Reference dipole EEG and estimated dipole EEG of Model 3 with different conductivity noises (variance, Var.). (A) Var. = 0.005. (B) Var. = 0.01. (C) Var. = 0.015. (D) Var. = 0.02. (E) Var. = 0.025. (F) Var. = 0.03. (G) Var. = 0.035 (H) Var. = 0.04 (I) Var. = 0.045 (J) Var. = 0.05 (K) Var. = 0.06 (L) Var. = 0.07 (M) Var. = 0.08 (N) Var. = 0.09 (O) Var. = 0.1. Red curve is the reference dipole EEG and the blue one is the estimated dipole EEG.

Table 5-4: Numerical analysis of the conductivity noise study

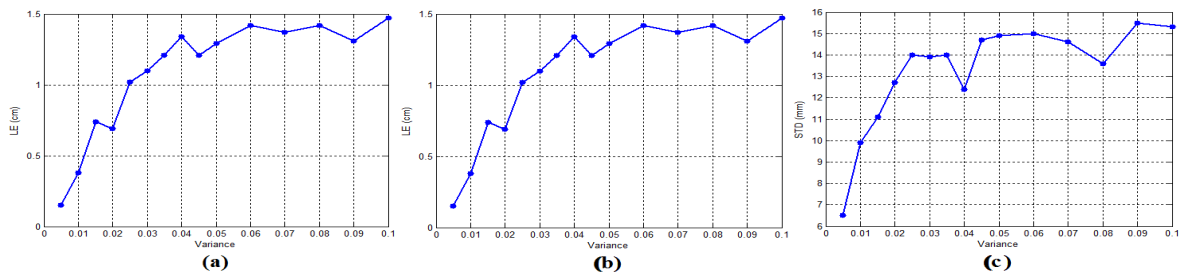| Variances	Estimated Positions	LE (cm)	Estimated Moments	OE (deg)	RE$_{diff}$ (%)	STD (mm)
0.005	(0.0471, 0.0535)	0.15	(0.0072, 0.0859)	0.0836	16.37	6.5
0.010	(0.0466, 0.0512)	0.38	(0.0069, 0.0755)	0.7384	25.70	9.9
0.015	(0.0469, 0.0476)	0.74	(0.0121, 0.0093)	0.9155	35.88	11.1
0.020	(0.0469, 0.0464)	0.69	(0.0054, -0.0011)	1.7718	39.65	12.7
0.025	(0.0467, 0.0440)	1.02	(0.0037, 0.0007)	1.3838	42.51	14.0
0.030	(0.0465, 0.0432)	1.10	(0.0062, 0.0257)	0.2367	45.52	13.9
0.035	(0.0473, 0.0424)	1.21	(-0.0056, 0.0193)	0.2824	46.84	14.0
0.040	(0.0463, 0.0417)	1.34	(0.0107, 0.0387)	0.2697	47.71	12.4
0.045	(0.0475, 0.0428)	1.21	(-0.0276, -0.0138)	2.0344	47.28	14.7
0.050	(0.0464, 0.0428)	1.29	(-0.0011, -0.0029)	2.7790	48.29	14.9
0.060	(0.0467, 0.0442)	1.42	(0.0014, 0.0008)	1.0517	49.93	15.0
0.070	(0.0486, 0.0421)	1.37	(-0.0024, -0.0061)	2.7668	50.49	14.6
0.080	(0.0477, 0.0416)	1.42	(0.0004, 0.0002)	1.1071	51.38	13.6
0.090	(0.0480, 0.0406)	1.31	(0.0056, 0.0054)	0.8036	52.39	15.5
0.100	(0.0472, 0.0403)	1.47	(-0.0034, -0.0006)	1.7455	53.26	15.3

Figure 5.10 (a) LE, (b) OE and (c) STD for Model 3 with different conductivity noises.

5.3 Segmentation effect study

To analyze the results of the segmentation effect study, the software called ParaView was used to visualize these results. Figure 5.16 to Figure 5.19 are the outputs. Figure 5.16 and Figure 5.17 show the top view and side view of grey matter and the region of interest. They are coloured by the goal function. According to the Dice's coefficients, segmentation done by threshold 0.4 and threshold 0.5 are almost the same. Thereby, the results based on threshold 0.5 were shown here.
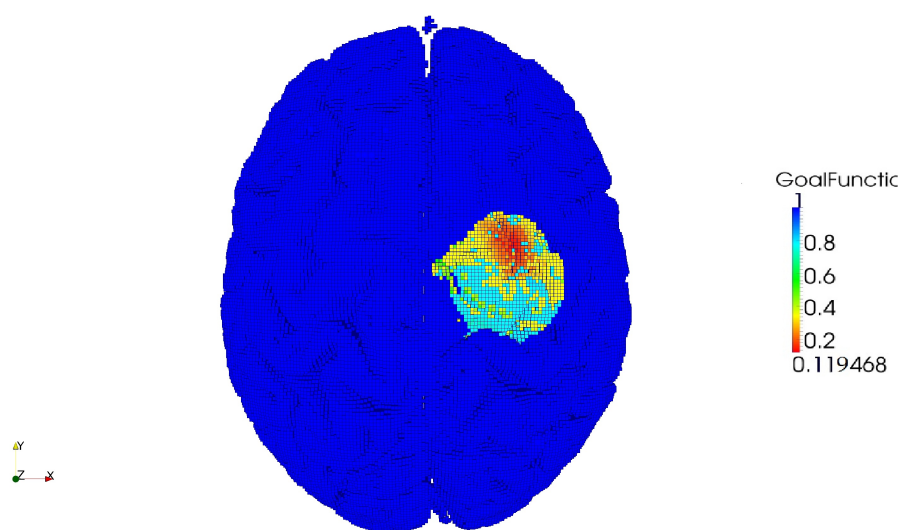

Figure 5.16 The top view of the grey matter and the region of interest for threshold 0.3.
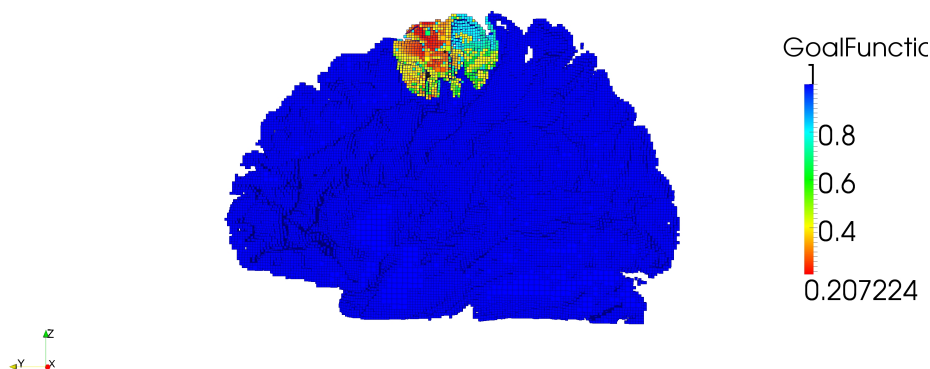

Figure 5.17 The side view of the grey matter and the region of interest for threshold 0.5.

Figure 5.18 and Figure 5.19 are the visualization of the initial dipole and the estimated dipole for the models with threshold 0.3 and threshold 0. In these two figures, the black arrow is the real dipole and the red one is the estimated dipole. The localization error given by the model with threshold 0.3 is 0.0129 and the relative error is 11.95%. For the model with threshold 0.5, the distance error is 0.0142 and the relative error is 20.72%. Table 5-5 lists the estimated dipole positions, the distance errors and the relative errors of the two models.
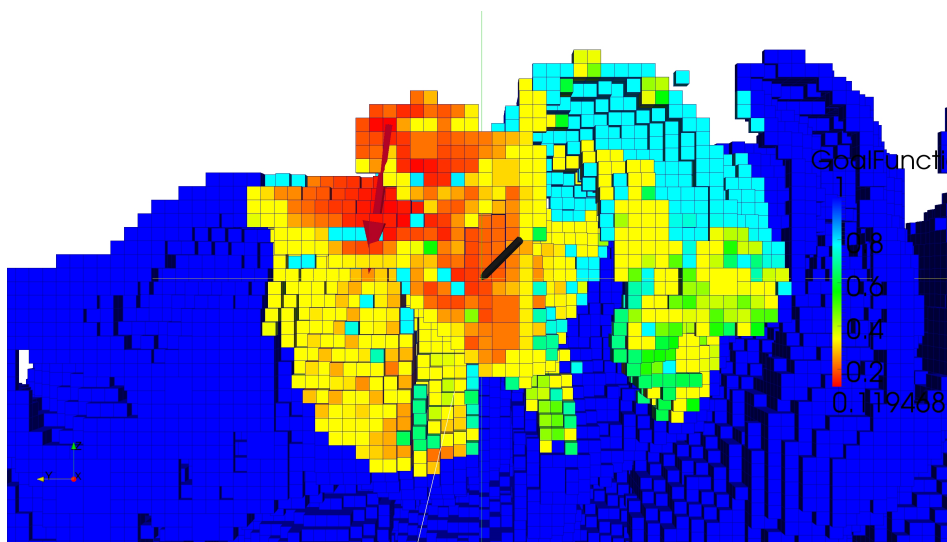

Figure 5.18 The reference dipole and the estimated dipole for threshold 0.3. The black arrow is the reference dipole and the red one is the estimated dipole.
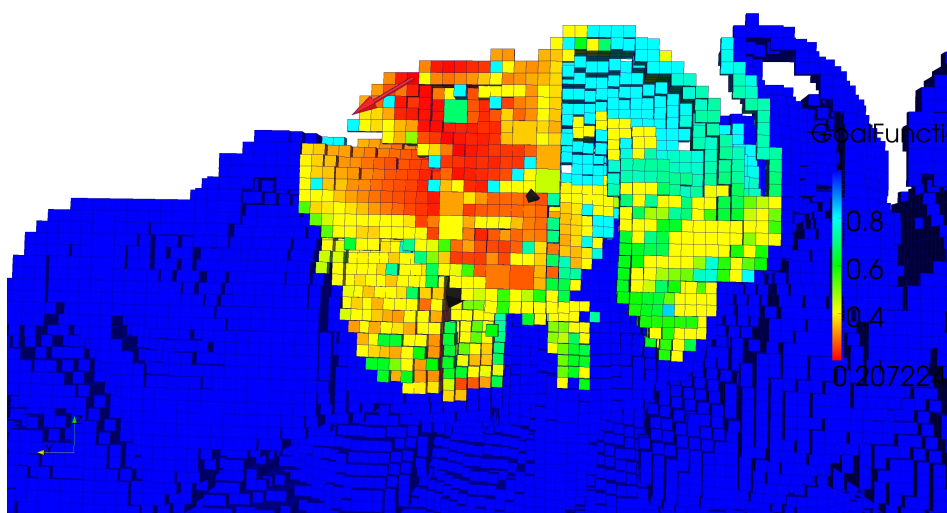

Figure 5.19 The reference dipole and the estimated dipole for threshold 0.5. The black arrow is the reference dipole and the red one is the estimated dipole.

Table 5-5: Estimated positions and errors of different segmentation models

Models	Dipole Positions	Localization Errors (m)	Relative Errors (%)
Reference	(0.1125, 0.1100, 0.1020)		
Model 1 (Threshold = 0.3)	(0.1145, 0.1195, 0.1105)	0.0129	11.95
Model 2 (Threshold = 0.5)	(0.1125, 0.1205, 0.1115)	0.0142	20.72

Figure 5.20 is the electrode errors for the two models. In these two figures, the blue curve is the reference EEG and the red one is the estimated EEG. The two curves match better in threshold 0.3 model than in threshold 0.5 model.
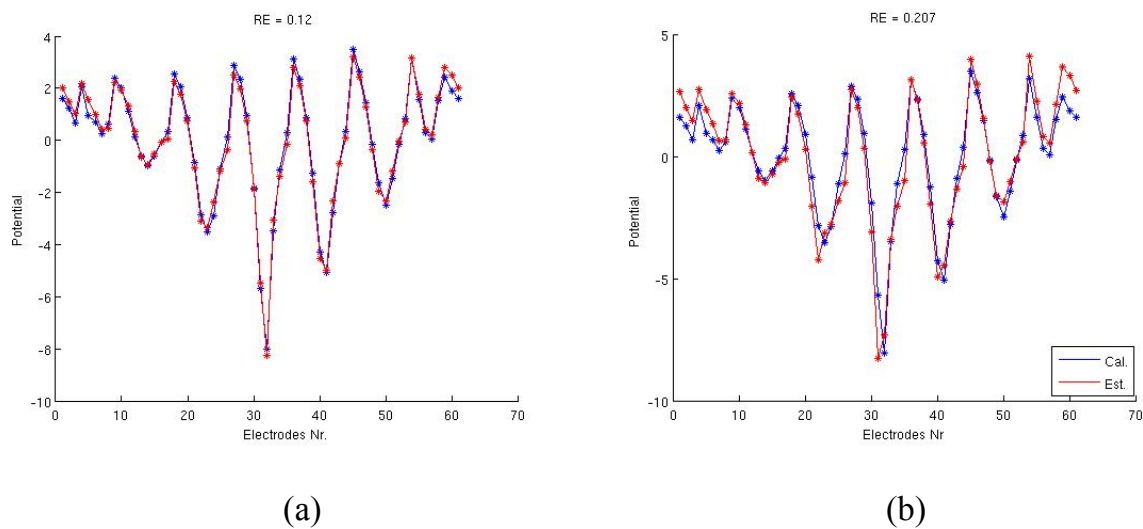

(a)   (b)

Figure 5.20 The electrode errors for (a) Threshold 0.3 and (b) Threshold 0.5. The blue curve is the potentials for reference model and the red one is the potentials for the estimated model. RE indicates the relative error.

From the above figures, it is evident that the model with threshold 0.5 has different potentials to that of the reference model which in turn gives errors in source localization. The model with threshold 0.3 has negligible error and proves to be good in source localization.

CHAPTER 6 DISCUSSIONS AND CONCLUSIONS

According to the different tissue models' study, head model plays an important role in EEG source localization. Both the forward problem (potentials of the same dipole in different models) and the inverse problem (goal functions of different models) gave high errors with the models with modified CSF in tissue study. Thereby, CSF is a significant tissue and should be paid more attention than other tissues.

The results of the signal noise study also gave the importance of the head models. This study also showed the acceptable signal noise range. Based on the simulated results, when the SNR value is higher than 25, the errors are acceptable. This means that in practice, the EEG measurement should be done in an environment which is not impacted by many noises. Better solution is to apply some de-noising techniques on the EEG signal to improve the SNR value.

From the conductivity study, the following conclusions can be made. Compared with other tissues, skin and skull are more sensitive to conductivity noise. More useful information given by this study is the acceptable noise range. The results indicated that if the variance is no bigger than 0.0025, all the results are considered accurate. With the increase in variance value, the relative errors become too high that cannot be accepted while the localization errors can still be considered as accurate until the variance value is higher than 0.0025. This means that the relative error is more sensitive to conductivity noise than the localization error.

As the model with threshold equal to 0.3 has less relative error and less localization error than the model with threshold 0.5, it proves to be good in source localization.

References

[1] J. C. De Munck. (1988, July). "The potential distribution in a layered anisotropic spheroidal volume conductor." *Journal of Applied Physics.* 64 (2) 464–470.

[2] S. van den Broeh, H. Zhou, M. Peters. (1996). "Computation of neuromagnetic fields using finite-element method and Biot-Savart law." *Medical and Biological Engineering and Computing.* 34 (1) 21–26.

[3] F. Edelvik, B. Andersson, S. Jakobsson, S. Larsson, M. Persson, Y. Shirvany. "An improved method for dipole modeling in EEG-based source localization." World Congress on Medical Physics and Biomedical Engineering, Munich, Germany, 2009.

[4] Hans Hallez, Bart Vanrumste, Roberta Grech, Joseph Muscat, Wim De Clercq, Anneleen Vergult, Yves D'Asseler, Kenneth P Camilleri, Simon G Fabri, Sabine Van Huffel and Ignace Lemahieu. (2007, Jan.). "Review on solving the forward problem in EEG source analysis." *Journal of NeuroEngineering and Rehabilitation.* [Online]. 4(46). Available: http://www.jneuroengrehab.com/content/4/1/46 [Jan. 13, 2012]

[5] Federica Vatta, Fabio Meneghini, Fabrizio Esposito, Stefano Mininel and Francesco Di Salle. (2009, June). "Realistic and Spherical Head Modeling for EEG Forward Problem Solution: A Comparative Cortex-Based Analysis." *Computational Intelligence and Neuroscience.* [Online]. 2010(13), pp. 123-134. Available: http://www.hindawi.com/journals/cin/2010/972060/#B1 [Jan. 13, 2012]

[6] http://ese.nju.edu.cn/bme/bioe-course/pdf/IEEEBME99.pdf

[7] Olivier de Weck and Il Yong Kim. 16.810. Class Lecture, Topic: "Finite Element Method." 33-218, Aeronautics and Astronautics, Massachusetts Institute of Technology, Cambridge, Massachusetts, Jan. 12, 2004.

[8] S.S. Bhavikatti. (2010, January 1). *Finite Element Analysis.* (2nd edition). [Online]. Available: http://www.newagepublishers.com/samplechapter/000973.pdf [Jan. 16, 2012]

[9] "Finite element method." Internet: http://en.wikipedia.org/wiki/Finite_element_method, Jan. 30, 2012 [Jan. 16, 2012]

[10] "Industrial Applications of the Finite Element Method." Internet: http://comp.uark.edu/~jjrencis/femur/Learning-Modules/Industrial-Applications-Of-Finite-Element-Analysis/ [Jan. 16, 2012]

[11] Mike Barton and S. D. Rajan. Class Lecture, Topic:"Finite Element Primer for

Engineers." Civil and Environmental Engineering, Arizona State University, Tempe, Arizona, 2000

[12] Roberta Grech, Tracey Cassar, Joseph Muscat, Kenneth.P.Camilleri, Simon.G.Fabri, Michalis Zervakis, Petros Xanthopoulos, Vangelis Sakkalis and Bart Vanrumste. (2008, June). "Review on solving the inverse problem in EEG source analysis." *Journal of NeuroEngineering and Rehabilitation*. [Online]. 5(25). Available: http://www.jneuroengrehab.com/content/5/1/25 [Oct. 24, 2011]

[13] Geertjan Huiskamp. (2008, Jan.). "Interindividual variability of skull conductivity: an EEG-MEG analysis." *International Journal of Bioelectromagnetism*. [Online]. 10(1), pp. 25-30. Available: http://ijbem.k.hosei.ac.jp/volume10/number1/100104.pdf [Jan. 23, 2012]

[14] Federica Vatta, Paolo Bruno and Paolo Inchingolo. (2002, Jan.). "Improving Lesion Conductivity Estimate by Means of EEG Source Localization Sensitivity to Model Parameter." *Journal of Clinical Neurophysiology*. [Online]. 19(1), pp. 1-15. Available: http://www.tbs.ts.it/PUBLIC/archives/EEG-18.pdf [Jan. 23, 2012]

[15] M. R. Bashar, Y. Li, P. Wen. (2009, Oct.). "Uncertainty and sensitivity analysis for anisotropic inhomogeneous head tissue conductivity in human head modeling." *Australasian Physical & Engineering Sciences in Medicine*. [Online]. 33(2), pp. 145-152. Available: http://www.springerlink.com/content/ah7768p0468tw420/fulltext.pdf [Jan. 23, 2012]

[16] Zhigang Peng. "Segmentation of White Matter, Gray Matter, and CSF from MR Brain Images and Extraction of Vertebrae from MR Spinal Images." Ph.D. dissertation, University of Cincinnati, USA, 2006.

[17] http://publications.lib.chalmers.se/records/fulltext/125991.pdf

[18] Y. Shirvany. "Non-invasive EEG Functional Neuroimaging for Localizing Epileptic Brain Activity, Licentiate of Engineering." PhD report, Chalmers University of Technology, Göteborg, Sweden, 2012.

[19] http://niremf.ifac.cnr.it/tissprop/

[20] "FMRIB Software Library." Internet: http://www.fmrib.ox.ac.uk/fsl/, Aug., 2008 [Oct. 26, 2011]

[21] S.M. Smith, M. Jenkinson, M.W. Woolrich, C.F. Beckmann, T.E.J. Behrens, H. Johansen-Berg, P.R. Bannister, M. De Luca, I. Drobnjak, D.E. Flitney, R. Niazy, J. Saunders, J. Vickers, Y. Zhang, N. De Stefano, J.M. Brady, and P.M. Matthews. "Advances in functional and structural MR image analysis and implementation as FSL." *NeuroImage*. [Online]. 23(S1), pp.208-219. Available:

http://www.sciencedirect.com/science?_ob=MiamiImageURL&_cid=272508&_user=646099&_pii=S1053811904003933&_check=y&_origin=search&_coverDate=31-Dec-2004&view=c&wchp=dGLbVlS-zSkzk&md5=c344d102d30c165dc7c0373d419e9d16/1-s2.0-S1053811904003933-main.pdf. [Oct. 26, 2011]

[22] "Segmentation Validation Engine." Internet: http://sve.loni.ucla.edu/instructions/metrics/dice/ [Jan. 16, 2012]

[23] E. Kosman and K. J. Leonard. (2004, Aug.). "Similarity coefficients for molecular markers in studies of genetic relationships between individuals for haploid, diploid, and polyploid species." *Molecular Ecology.* [Online]. 14(2), pp. 415-424. Available: http://afrsweb.usda.gov/SP2UserFiles/ad_hoc/36400500Publications/KJL/sim_coef.pdf [Jan. 16, 2012]